Acta Crystallographica Section F
Structural Biology and Crystallization Communications
ISSN 1744-3091

Crystallization of Doc and the Phd–Doc toxin–antitoxin complex

Abel Garcia-Pino,[a,b]* Minh-Hoa Dao-Thi,[a,b] Ehud Gazit,[c] Roy David Magnuson,[d] Lode Wyns[a,b] and Remy Loris[a,b]

[a]Laboratorium voor Ultrastructuur, Vrije Universiteit Brussel, Pleinlaan 2, B-1050 Brussel, Belgium, [b]Department of Molecular and Cellular Interactions, Vrije Universiteit Brussel, Pleinlaan 2, B-1050 Brussel, Belgium, [c]Department of Molecular Microbiology and Biotechnology, Tel Aviv University, Tel Aviv 69778, Israel, and [d]Department of Biological Sciences, University of Alabama in Huntsville, Huntsville, AL 35899, USA

Correspondence e-mail: agarciap@vub.ac.be

Received 8 August 2008
Accepted 1 October 2008

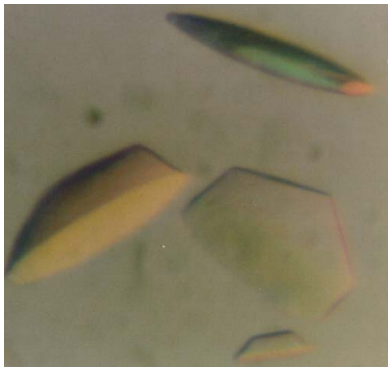

The *phd*/*doc* addiction system is responsible for the stable inheritance of lysogenic bacteriophage P1 in its plasmidic form in *Escherichia coli* and is the archetype of a family of bacterial toxin–antitoxin modules. The His66Tyr mutant of Doc (Doc^{H66Y}) was crystallized in space group $P2_1$, with unit-cell parameters a = 53.1, b = 198.0, c = 54.1 Å, β = 93.0°. These crystals diffracted to 2.5 Å resolution and probably contained four dimers of Doc in the asymmetric unit. Doc^{H66Y} in complex with a 22-amino-acid C-terminal peptide of Phd ($Phd^{52\text{-}73Se}$) was crystallized in space group $C2$, with unit-cell parameters a = 111.1, b = 38.6, c = 63.3 Å, β = 99.3°, and diffracted to 1.9 Å resolution. Crystals of the complete wild-type Phd–Doc complex belonged to space group $P3_121$ or $P3_221$, had an elongated unit cell with dimensions $a = b$ = 48.9, c = 354.9 Å and diffracted to 2.4 Å resolution using synchrotron radiation.

1. Introduction

Toxin–antitoxin (TA) modules are a class of operons that are widespread in free-living and opportunistic pathogenic prokaryotes (Pandey & Gerdes, 2005). They are involved in regulating the pace of metabolism and may induce a state of dormancy during nutritional stress (Pedersen *et al.*, 2002; Gerdes *et al.*, 2005). In a few cases, a link between TA modules and persister cell formation has been found (Keren *et al.*, 2004; Lewis, 2005). Under certain conditions, ectopic overexpression of TA modules may lead to cell death (Amitai *et al.*, 2004; Kolodkin-Gal & Engelberg-Kulka, 2006; Engelberg-Kulka *et al.*, 2006), although this notion has been contested (Pedersen *et al.*, 2002; Gerdes *et al.*, 2005) and high-level protein production after induction of TA proteins remains possible if the mRNA lacks a cleavage site for the RNase toxin (Suzuki *et al.*, 2005). On plasmids, TA modules act as addiction systems aiding plasmid maintenance in the bacterial population (Gerdes *et al.*, 1986). Related effects have been observed for chromosome-located TA systems as some of them have been shown to diminish large-scale genome reductions in the absence of selection (Szekeres *et al.*, 2007).

TA modules have been categorized into a number of families based upon sequence similarities between their respective toxins and antitoxins (Pandey & Gerdes, 2005; Anantharaman & Aravind, 2003). Where investigated, the toxins have been shown to be mRNA-cleaving RNases (Christensen & Gerdes, 2003; Christensen *et al.*, 2003; Pedersen *et al.*, 2003; Zhang, Zhang, Hoeflich *et al.*, 2003; Kamada & Hanaoka, 2005) or non-enzymatic ribosome inhibitors (Liu *et al.*, 2008) or to poison gyrase (Bernard & Couturier, 1992; Jiang *et al.*, 2002). Structural studies have identified several different toxin folds (Loris *et al.*, 1999; Hargreaves *et al.*, 2002; Takagi *et al.*, 2005; Kamada & Hanaoka, 2005; Mattison *et al.*, 2006). Among the best known is a microbial ribonuclease fold that has been found in mRNA interferases such as RelE, YoeB and HigB and also in the gyrase poison ParE. Similarly, the MazF mRNA-interferase family and the gyrase poison CcdB share a common fold (Hargreaves *et al.*, 2002; Buts *et al.*, 2005). All antitoxins show a modular structure (Loris *et al.*, 2003; Kamada *et al.*, 2003; Madl *et al.*, 2006; Mattison *et al.*, 2006; Oberer *et al.*, 2007; Li *et al.*, 2008), in agreement with genetics, that pinpoints DNA-binding activity at their N-terminal region and toxin-neutralizing activity at their C-terminal region (Smith & Magnuson,

Table 1
Biophysical parameters.

	No. of amino acids	Molecular weight (Da)	Extinction coefficient at 280 nm (M^{-1} cm^{-1})
Doc	126	13588.2	5960
Doc^{H66Y}	137	14762.5	7450
Phd	73	8133.1	1490
Phd$^{52\text{-}73Se}$	22	2592.5	—

2004; McKinley & Magnuson, 2005; Madl *et al.*, 2006; Zhang, Zhang & Inouye, 2003). Recent genetic evidence also suggests that toxins belonging to one family may be associated with different antitoxin DNA-binding domains (Fico & Mahillon, 2006), complicating the genetic relationships between different families of TA modules.

The *phd*/*doc* operon forms a relatively small family of TA modules, the first member of which was identified on bacteriophage P1, where it stabilizes the prophage in its plasmidic form (Lehnherr *et al.*, 1993). Like other TA modules, *phd*/*doc* encodes a toxin (Doc) preceded by an antitoxin (Phd). The members of the Phd protein family show weak sequence identity to the YefM family of antitoxins (Anantharaman & Aravind, 2003; Kamada & Hanaoka, 2005). The N-terminal domain of Phd is a DNA-binding domain that is essential for autoregulation, although efficient repression also requires the presence of Doc (Magnuson *et al.*, 1996; Magnuson & Yarmolinsky, 1998; Gazit & Sauer, 1999*a*). The C-terminal domain of the protein is responsible for counteracting Doc (Smith & Magnuson, 2004; McKinley & Magnuson, 2005).

ClpXP-mediated degradation of Phd upon plasmid loss activates Doc (Lehnherr & Yarmolinsky, 1995). Doc interferes with basic metabolism at the level of translation by an action that mimics that of the antibiotic hygromycin B (Liu *et al.*, 2008). The molecular mechanism behind this action remains unknown. Analytical studies have suggested that the complex between Phd and Doc has a 2:1 stoichiometry (Gazit & Sauer, 1999*b*). Evidence from CD spectroscopy suggested changes in secondary structure upon complex formation (Gazit & Sauer, 1999*b*), in agreement with observations on other TA systems that the intrinsically flexible C-terminus of the antitoxin protein becomes folded upon binding to the toxin (Loris *et al.*, 2003; Kamada *et al.*, 2003; Kamada & Hanaoka, 2005; Takagi *et al.*, 2005; Mattison *et al.*, 2006). Here, we report the crystallization of Doc and of the Phd–Doc complex from bacteriophage P1.

2. Material and methods

2.1. Expression and purification of Doc^{H66Y}

The biophysical parameters used for Doc, Doc^{H66Y}, Phd and Phd$^{52\text{-}73Se}$ were derived from their primary sequences and are given in Table 1. The oligonucleotides agDOC5a (CCCCATATGAGGCATATATCACCGGAAGAAC) and agDOC5d (CCCCTCGAGCGGATCCGCAGAACCATACAATC) were used to amplify *docH66Y* from a *malE-docH66Y* construct (Magnuson & Yarmolinsky, 1998) by PCR, while at the same time introducing *Nde*I and *Xho*I restriction sites. After digesting this PCR product with *Nde*I and *Xho*I, the fragment containing the *docH66Y* gene was inserted into a pET21b vector (Novagen), which places a six-His tag at the C-terminus of *docH66Y*. *Escherichia coli* BL21 (DE3) cells were subsequently transformed with pET21b-docH66Y. Cell cultures were grown in LB medium at 310 K until the OD at 600 nm was between 0.6 and 0.8. Expression of the *docH66Y* gene was then induced by adding 1 m*M* isopropyl β-D-1-thiogalactopyranoside (IPTG). 2 h after induction, the cells were harvested by centrifugation and subsequently resuspended in 20 m*M* Tris–HCl pH 8.0, 1 m*M* EDTA, 0.1 mg ml^{-1} 4-(2-aminoethyl)benzenesulfonylfluoride hydrochloride (AEBSF) and 1 mg ml^{-1} leupeptin. Cells were broken at 277 K by passage through a cell cracker and cell debris was removed by centrifugation. The protein was loaded onto a Ni–NTA affinity column equilibrated in 20 m*M* Tris–HCl pH 8.0. The bound protein was eluted with a ten column-volume linear gradient of imidazole (0–1 *M*) in 250 m*M* NaCl. Fractions containing Doc^{H66Y} were collected and further purified on a Superdex 75 HR gel-filtration column (Amersham Biosciences) previously equilibrated with 20 m*M* Tris–HCl pH 8.0. The purity of the sample was analyzed by running a 10% SDS–PAGE gel and the identity of the protein was confirmed by N-terminal sequencing (the first ten residues of the protein were sequenced and the obtained sequence was a perfect match with that expected for Doc) and Western blotting using antibodies raised in rabbits against the Phd–Doc complex (Fig. 1).

2.2. Preparation of complexes

The wild-type Phd–Doc complex was purified according to Gazit & Sauer (1999*b*). Phd$^{52\text{-}73Se}$, the C-terminal 22 amino acids of Phd with selenomethionine substituted for Leu52 and Leu70, was obtained from Alta Bioscience (Birmingham, England). The Doc^{H66Y}–Phd$^{52\text{-}73Se}$ complex was prepared by adding equimolar amounts of Phd$^{52\text{-}73Se}$ to a concentrated Doc^{H66Y} solution without further purification. Because of the low molar extinction coefficient of the peptide, it was not possible to measure its concentration spectrophotometrically. Therefore, 1.0 mg lyophilized powder (assumed to be pure) was weighed on a microbalance and dissolved directly in the solution containing Doc^{H66Y}.

2.3. Crystallization

Crystallization conditions were screened at 293 K with the hanging-drop vapour-diffusion method using Hampton Crystal Screens 1 and 2 (Hampton Research, Riverside, California, USA; Jancarik & Kim, 1991). For crystallization experiments involving

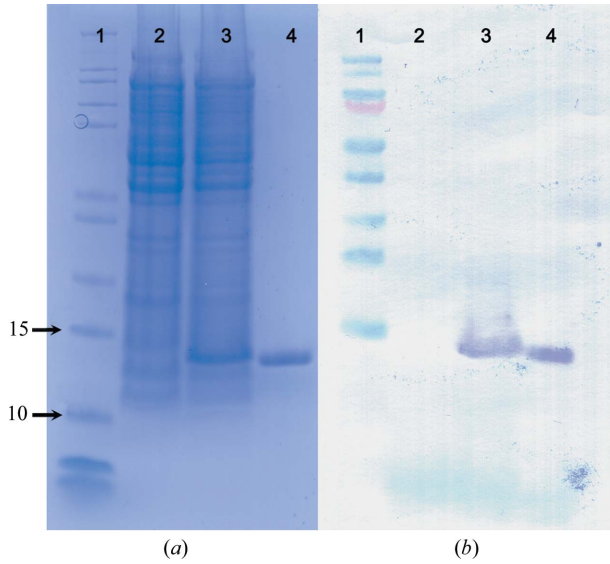

Figure 1
Purification of Doc^{H66Y}. (*a*) Coomassie-stained SDS–PAGE of the affinity chromatography fractions. Lane 1, molecular-weight markers (kDa); lane 2, soluble protein before induction; lane 3, soluble protein 2 h after induction; lane 4, Doc^{H66Y} after purification on the His-trap affinity column. (*b*) Identification of Doc^{H66Y} on a Western blot developed with rabbit antibodies directed against wild-type Doc. The lanes are equivalent to those in (*a*).

Doc^{H66Y}, the protein was dialyzed against 20 m*M* Tris–HCl pH 8.0 and concentrated to 10 mg ml^{-1}. Concentrations were estimated spectrophotometrically at 280 nm using a theoretical molar extinction coefficient of 7450 M^{-1} cm^{-1} calculated from the amino-acid sequence (Gill & von Hippel, 1989). The Doc^{H66Y}–Phd$^{52\text{-}73Se}$ complex was concentrated to 10 mg ml^{-1} in 20 m*M* Tris–HCl pH 7.5 (a 1:1 stoichiometry was assumed, corresponding to a calculated molar extinction coefficient of 7450 M^{-1} cm^{-1}). The wild-type Phd–Doc complex was concentrated to 5 mg ml^{-1} in 50 m*M* Tris–HCl pH 7.4 (a 2:1 Phd:Doc stoichiometry was assumed, corresponding to a theoretical molar extinction coefficient of 8940 M^{-1} cm^{-1} for the complex). Drops consisting of 2 µl protein solution and 2 µl precipitant solution were equilibrated against 500 µl precipitant solution. Promising conditions were further optimized by varying the precipitant concentration, the temperature, the pH and the ratio of protein to precipitant solution in the drops.

Seeding of Doc^{H66Y} was performed by diluting 1 µl of a drop containing small crystals into 50 µl precipitant solution, which was followed by vortexing and centrifugation (5 min at 13 000 rev min^{-1} in an Eppendorf centrifuge; approximately 100*g*) to eliminate large pieces of crystals and retain only the nuclei. 1 µl of the supernatant was serially diluted into precipitant solution consisting of 100 m*M* Tris–HCl pH 8.0, 20% PEG 10 000 (10–10^8-fold dilution, with the optimal dilution being 10^6–10^7-fold). 0.3 µl of these dilutions was used as an additive in the crystallization setups (which consisted of 2 µl protein solution and 2 µl precipitant solution). The protein concentration was lowered to 5 mg ml^{-1}, a concentration at which spontaneous nucleation was not observed within several weeks.

2.4. Data collection

A search for a suitable cryoprotectant solution for the Doc^{H66Y} crystals was not successful. Crystals of Doc^{H66Y} were therefore mounted in thin-walled glass capillaries and X-ray data were collected at room temperature on the EMBL beamline X13 of the DESY synchrotron (Hamburg, Germany) using a 165 mm MAR CCD detector.

Data for the Doc^{H66Y}–Phd$^{52\text{-}73Se}$ complex were collected on EMBL beamline X12 of the DESY synchrotron using a 225 mm MAR CCD detector. The crystals were flash-frozen directly in the cryostream after a brief transfer (30–60 s) to a cryoprotectant solution consisting of 100 m*M* Tris–HCl pH 8.5, 200 m*M* NaCl, 1.5 *M* NaBr and 35% MPD.

Crystals of the Phd–Doc complex were frozen directly in the cryostream without any additional cryoprotectant. Data were initially measured to 3.2 Å resolution on EMBL beamline BW7B of the DESY synchrotron using a MAR 345 image plate. Subsequently, higher resolution data were collected from the same crystal on beamline ID14-1 of the ESRF synchrotron (Grenoble, France) using an ADSC Quantum-4 detector (using two passes at 2.9 and 2.4 Å resolution in order to compensate for overloads) and merged with the DESY data in order to compensate for the loss of low-resolution reflections owing to overloads. Separating reflections along c^* ultimately limited the useful resolution limit to 2.4 Å. The mosaicity of this crystal was 0.15°, which was much better than the typical 1.0° observed for other tested crystals of the Phd–Doc complex.

Because the long *c* axis of these crystals runs perpendicular to the plane of the plate-shaped crystals, it was not possible to orient the Phd–Doc crystals with their *c* axis parallel to the spindle axis (which would have minimized both the spatial overlap and the rotation range necessary to obtain a complete data set). Therefore, prior to data collection the crystal was oriented such that its *c* axis was roughly perpendicular to the direct-beam direction. From this orientation, the crystal was rotated 55° back in φ and 110° of data were then collected. This strategy allowed us to avoid the crystal orientations with the most severe overlap problems while still obtaining an essentially complete data set.

All data were indexed and integrated using *DENZO* and subsequent scaling and merging were performed using *SCALEPACK* (Otwinowski & Minor, 1997). Intensities were converted to structure-factor amplitudes using the *CCP*4 program *TRUNCATE* and the program *MATTHEWS_COEF* was used to calculated Matthews coefficients for cell-content analysis (Collaborative Computational Project, Number 4, 1994). Self-rotation function analysis was performed using *MOLREP* (Vagin & Teplyakov, 1997).

For phasing, a crystal was soaked for about 3 min in a cryoprotectant solution (0.2 *M* NaCl, 0.1 *M* sodium acetate pH 4.6 and 35% MPD) enriched with 1.5 *M* NaBr. Data were collected at the Br *K* edge and processed using *DENZO* and *SCALEPACK* (Otwinowski & Minor, 1997). The heavy-atom substructure was determined with *SHELXD* (Sheldrick, 2008) and phasing subsequently proceeded with *SHARP* (de La Fortelle & Bricogne, 1997) as combined in the *AutoRickshaw* pipeline (Panjikar *et al.*, 2005).

3. Results and discussion

Because of problems in producing wild-type Doc in large quantities arising from the toxic nature of the protein (its action is to block protein synthesis by inhibiting the ribosome), we decided to use the less toxic variant His66Tyr (Magnuson & Yarmolinsky, 1998). Size-exclusion analysis of the mutant His66Tyr (Doc^{H66Y}) preparation that

(*a*) (*b*) (*c*) (*d*)

Figure 2
Different crystals of free Doc^{H66Y} and its complexes with Phd. (*a*) Initial crystals obtained of free Doc^{H66Y}. (*b*) Large crystals of free Doc^{H66Y} obtained after seeding. (*c*) Monoclinic crystals of Doc^{H66Y}–Phd$^{52\text{-}73Se}$. (*d*) Hexagonal crystal form of the Phd–Doc complex. The scale bar corresponds to 0.1 mm.

eluted from the Ni–NTA affinity column showed two peaks with apparent molecular weights corresponding to a dimer and a monomer. The ratio between monomer and dimer depended heavily on the pH: the dimer was stable only at pH 8.0 and above (data not shown). Both forms were used for crystallization, but crystals were only obtained using the dimer of Doc^{H66Y}. Initial crystals of the Doc^{H66Y} dimer were obtained in 20% PEG 10 000, 100 m*M* Tris–HCl pH 8.0 (Fig. 2*a*). These crystals were improved further by microseeding, resulting in large single crystals (Fig. 2*b*) that were suitable for X-ray diffraction experiments. They belonged to space group $P2_1$, with unit-cell parameters $a = 53.1$, $b = 198.0$, $c = 54.1$ Å, $\beta = 93.0^\circ$, and typically diffracted to 2.5 Å resolution. The statistics for data collection are given in Table 2. Analysis of the unit-cell content (Matthews, 1968) assuming the presence of discrete dimers suggested that the asymmetric unit contained between three and five Doc^{H66Y} dimers (with V_M values of 3.21, 2.40 and 1.92 Å^3 Da^{-1} for three, four or five dimers in the asymmetric unit, corresponding to 62%, 49% and 36% solvent, respectively). The $\kappa = 180^\circ$ section of the self-rotation function only showed two pronounced peaks that were distinct from those corresponding to the crystallographic symmetry operations. Analysis of the native Patterson also showed a pronounced non-origin peak at $u = 0.473$, $v = 0.000$, $w = 0.499$. Together, these observations are consistent with the presence of two pairs of two dimers in the asymmetric unit that are related to each other through a purely translational operation. However, this conclusion remains tentative until the structure has been determined.

Crystals of the Doc^{H66Y}–$Phd^{52\text{-}73Se}$ complex (Fig. 2*c*) were obtained in 100 m*M* sodium acetate pH 4.6, 200 m*M* ammonium acetate, 30%(*w*/*v*) PEG 4000. The crystals grew as very thin plates of dimensions 0.3 × 0.2 × 0.01 mm (Fig. 2*c*). They belonged to space group *C*2, with unit-cell parameters $a = 111.1$, $b = 38.6$, $c = 63.3$ Å, $\beta = 99.3^\circ$. The best crystals diffracted to 1.9 Å resolution (Fig. 3*a*). Statistics for data collection are given in Table 2. Calculation of Matthews coefficients (Matthews, 1968) indicated that the asymmetric unit is most likely to contain two Doc^{H66Y}–$Phd^{52\text{-}73Se}$ complexes ($V_M = 1.92$ Å^3 Da^{-1} corresponding to a solvent content of 35.9% *versus* $V_M = 3.84$ Å^3 Da^{-1} and 68% solvent content for a single complex in the asymmetric unit). Analysis of the self-rotation function did not reveal any significant peaks apart from those expected from crystallographic symmetry.

After an initial phasing attempt using the selenomethionines present in the $Phd^{52\text{-}73Se}$ peptide failed (data not shown), a KBr soak

Table 2
Data-collection statistics.

Values in parentheses are for the highest resolution shell.

	Doc^{H66Y}	Doc^{H66Y}–$Phd^{52\text{-}73Se}$ (native)	Doc^{H66Y}–$Phd^{52\text{-}73Se}$ (Br soak)	Phd–Doc
Beamline	X13	BW7A	X12	ID14-1/BW7B
No. of passes	1	1	1	3
No. of images per pass	360	120	360	110
Mosaicity (°)	0.35	0.90	0.95	0.15
Wavelength (Å)	0.808	0.9778	0.9189	0.934
Resolution (Å)	15.0–2.45 (2.51–2.45)	15.0–1.90 (1.96–1.90)	15.0–1.90 (1.97–1.90)	42.00–2.40 (2.49–2.40)
Completeness (%)	99.7 (100)	99.7 (99.6)	99.7 (98.8)	98.1 (97.8)
No. of measured reflections	149537 (10116)	118336 (11052)	101249 (9809)	211763 (14440)
No. of unique reflections	40500 (3915)	24737 (2786)	21369 (2087)	19457 (1857)
$\langle I/\sigma(I)\rangle$	7.7 (2.2)	7.8 (3.5)	12.5 (4.1)	23.2 (10.8)
Redundancy	3.7	4.7	4.7	10.9
R_{merge}†	0.102 (0.53)	0.106 (0.46)	0.103 (0.616)	0.085 (0.224)
Resolution cutoff for SAD phasing (Å)	—	—	2.5	—
$\langle d''/\sigma\rangle$	—	—	1.32	—
CC_{all}	—	—	36.87	—
CC_{weak}	—	—	18.33	—
No. of heavy atoms found	—	—	17	—

† $R_{merge} = \sum_{hkl}\sum_i |I_i(hkl) - \langle I(hkl)\rangle| / \sum_{hkl}\sum_i I_i(hkl)$.

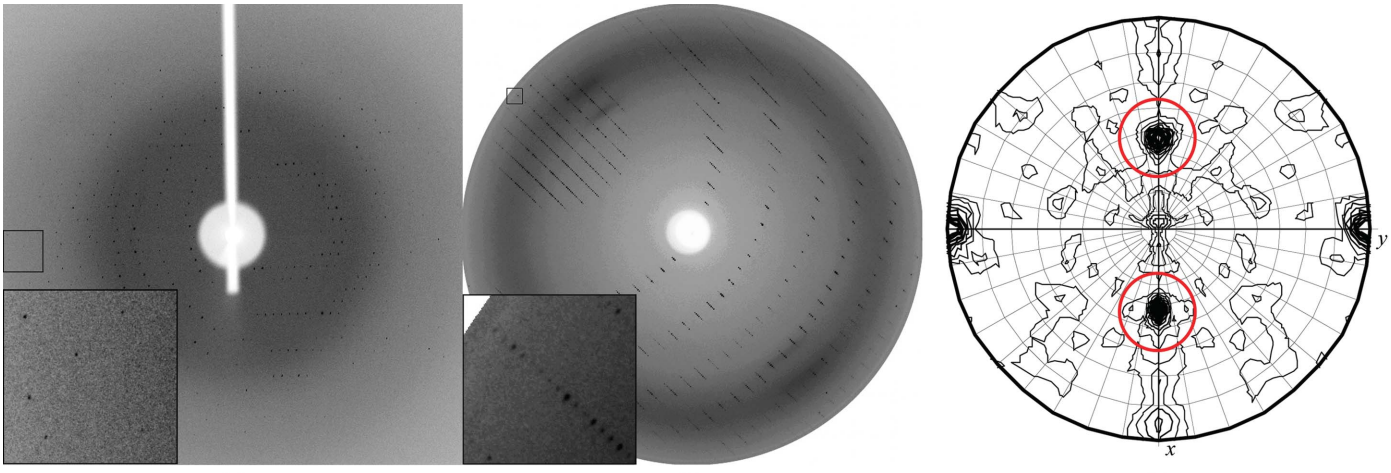

(*a*) (*b*) (*c*)

Figure 3
Typical diffraction patterns of (*a*) DocH66Y–$Phd^{52\text{-}73Se}$ and (*b*) Phd–Doc. In both cases the rotation angle is 1°. The inset in (*b*) shows a clear separation of the reflections in the *c** direction. (*c*) Self-rotation function with $\kappa = 180^\circ$ for Doc^{H66Y} crystals. Red circles indicate peaks corresponding to noncrystallographic symmetry axes.

was attempted. Using data collected at the Br *K* edge, a heavy-atom substructure consisting of 17 potential bromide ions (or seleniums from the peptide) was identified with *SHELXD* (Sheldrick, 2008). Subsequent automatic phasing with the *AutoRickshaw* pipeline (Panjikar *et al.*, 2005) resulted in an interpretable electron-density map showing two complexes in the asymmetric unit. Refinement of this structure is ongoing.

Crystals of the Phd–Doc complex (Fig. 2*d*) grew from 100 m*M* sodium acetate pH 4.5, 20 m*M* $CaCl_2$ and 35–40%(*v*/*v*) MPD. These crystals appeared after a few days and were shaped as halves of hexagonal plates (Fig. 2*d*). The crystals belonged to space group $P3_121$ or $P3_221$, with unit-cell parameters $a = b = 48.9$, $c = 354.9$ Å. A typical diffraction pattern is shown in Fig. 3(*b*). Although these crystals did not diffract on our home source, diffraction was systematically observed to at least 3.0 Å resolution using synchrotron radiation and the best crystal diffracted to at least 2.4 Å on ESRF beamline ID14-1. Statistics for the best native data that have been collected to date are given in Table 2. A Phd:Doc stoichiometry of 2:1 has previously been reported for the isolated complex (Gazit & Sauer, 1999*b*), but it is known that toxin–antitoxin complexes can have varying stoichiometries (Dao-Thi *et al.*, 2002; Monti *et al.*, 2007). Although SDS–PAGE analysis of the crystals indicates that both Doc and Phd are present in the crystals, it is difficult to pinpoint the exact stoichiometry and different ratios remain possible. Analysis of the self-rotation function of these crystals only showed pronounced peaks at $\kappa = 180^\circ$ and $\kappa = 120^\circ$ corresponding to the crystallographic symmetry axes, allowing no further conclusions to be drawn with respect to the entity present in the asymmetric unit. Fig. 3(*e*) only shows maxima corresponding to crystallographic symmetry. The crystal structures of other TA complexes have shown toxin–antitoxin stoichiometries of 2:1 for MazEF (Kamada *et al.*, 2003), 1:1 for archaeal RelBE and for a FitAB–DNA complex (Takagi *et al.*, 2005; Mattison *et al.*, 2006) and 1:2 for YoeB–YefM (Kamada & Hanaoka, 2005).

In conclusion, we obtained well diffracting crystals for the components of the *phd*/*doc* toxin–antitoxin module. Doc sequences show no evolutionary relationship to any other protein of known structure and its fold cannot be predicted. The crystal structures of Doc and the Phd–Doc complex are likely to shed further light on the molecular mode of action of Doc and the way it is regulated by Phd.

This work was supported by grants from OZR-VUB, VIB and FWO-Vlaanderen. The authors acknowledge the use of EMBL beamlines X12, X13 and BW7B (DESY, Hamburg, Germany) and ID14-1 (ESRF, Grenoble, France).

References

Amitai, S., Yassin, Y. & Engelberg-Kulka, H. (2004). *J. Bacteriol.* **186**, 8295–8300.

Anantharaman, V. & Aravind, L. (2003). *Genome Biol.* **4**, R81.

Bernard, P. & Couturier, M. (1992). *J. Mol. Biol.* **226**, 735–745.

Buts, L., Lah, J., Dao-Thi, M.-H., Wyns, L. & Loris, R. (2005). *Trends Biochem. Sci.* **30**, 672–679.

Christensen, S. K. & Gerdes, K. (2003). *Mol. Microbiol.* **48**, 1389–1400.

Christensen, S. K., Pedersen, K., Hansen, F. G. & Gerdes, K. (2003). *J. Mol. Biol.* **332**, 809–819.

Collaborative Computational Project, Number 4 (1994). *Acta Cryst.* D**50**, 760–763.

Dao-Thi, M.-H., Charlier, D., Loris, R., Maes, D., Messens, J., Wyns, L. & Backmann, J. (2002). *J. Biol. Chem.* **277**, 3733–3742.

Engelberg-Kulka, H., Amitai, S., Kolodkin-Gal, I. & Hazan, R. (2006). *PLoS Genet.* **2**, e135.

Fico, S. & Mahillon, J. (2006). *BMC Genomics*, **7**, 259.

Gazit, E. & Sauer, R. T. (1999*a*). *J. Biol. Chem.* **274**, 2652–2657.

Gazit, E. & Sauer, R. T. (1999*b*). *J. Biol. Chem.* **274**, 16813–16818.

Gerdes, K., Christensen, S. K. & Lobner-Olesen, A. (2005). *Nature Rev. Microbiol.* **3**, 371–382.

Gerdes, K., Rasmussen, P. B. & Molin, S. (1986). *Proc. Natl Acad. Sci. USA*, **83**, 3116–3120.

Gill, S. C. & von Hippel, P. H. (1989). *Anal. Biochem.* **182**, 319–326.

Hargreaves, D., Santos-Sierra, S., Giraldo, R., Sabariegos-Jareño, R., de la Cueva-Méndez, G., Boelens, R., Díaz-Orejas, R. & Rafferty, J. B. (2002). *Structure*, **10**, 1425–1433.

Jancarik, J. & Kim, S.-H. (1991). *J. Appl. Cryst.* **24**, 409–411.

Jiang, Y., Pogliano, J., Helinski, D. R. & Konieczny, I. (2002). *Mol. Microbiol.* **44**, 971–979.

Kamada, K. & Hanaoka, F. (2005). *Mol. Cell*, **19**, 497–509.

Kamada, K., Hanaoka, F. & Burley, S. K. (2003). *Mol. Cell*, **11**, 875–884.

Keren, I., Shah, D., Spoering, A., Kaldalu, N. & Lewis, K. (2004). *J. Bacteriol.* **186**, 8172–8180.

Kolodkin-Gal, I. & Engelberg-Kulka, H. (2006). *J. Bacteriol.* **188**, 3420–3423.

La Fortelle, E. de & Bricogne, G. (1997). *Methods Enzymol.* **276**, 472–494.

Lehnherr, H., Maguin, E., Jafri, S. & Yarmolinsky, M. B. (1993). *J. Mol. Biol.* **233**, 414–428.

Lehnherr, H. & Yarmolinsky, M. B. (1995). *Proc. Natl Acad. Sci. USA*, **92**, 3274–3277.

Lewis, K. (2005). *Biochemistry (Mosc.)*, **70**, 267–274.

Li, G. Y., Zhang, Y., Inouye, M. & Ikura, M. (2008). *J. Mol. Biol.* **380**, 107–119.

Liu, M., Zhang, Y., Inouye, M. & Woychik, N. A. (2008). *Proc. Natl Acad. Sci. USA*, **105**, 5885–5890.

Loris, R., Dao-Thi, M.-H., Bahassi, E. M., Van Melderen, L., Poortmans, F., Liddington, R., Couturier, M. & Wyns, L. (1999). *J. Mol. Biol.* **285**, 1667–1677.

Loris, R., Marianovsky, I., Lah, J., Laeremans, T., Engelberg-Kulka, H., Glaser, G., Muyldermans, S. & Wyns, L. (2003). *J. Biol. Chem.* **278**, 28252–28257.

Madl, T., Van Melderen, L., Mine, N., Respondek, M., Oberer, M., Keller, W., Khatai, L. & Zangger, K. (2006). *J. Mol. Biol.* **364**, 170–185.

Magnuson, R., Lehnherr, H., Mukhopadhyay, G. & Yarmolinsky, M. B. (1996). *J. Biol. Chem.* **271**, 18705–18710.

Magnuson, R. & Yarmolinsky, M. B. (1998). *J. Bacteriol.* **180**, 6342–6351.

Matthews, B. W. (1968). *J. Mol. Biol.* **33**, 491–497.

Mattison, K., Wilbur, J. S., So, M. & Brennan, R. G. (2006). *J. Biol. Chem.* **281**, 37942–37951.

McKinley, J. E. & Magnuson, R. D. (2005). *J. Bacteriol.* **187**, 765–770.

Monti, M. C., Hernández-Arriaga, A. M., Kamphuis, M. B., López-Villarejo, J., Heck, A. J., Boelens, R., Díaz-Orejas, R., van den Heuvel, R. H. (2007). *Nucleic Acids Res.* **35**, 1737–1749.

Oberer, M., Zangger, K., Gruber, K. & Keller, W. (2007). *Protein Sci.* **16**, 1676–1688.

Otwinowski, Z. & Minor, W. (1997). *Methods Enzymol.* **276**, 307–326.

Pandey, D. P. & Gerdes, K. (2005). *Nucleic Acids Res.* **33**, 966–976.

Panjikar, S., Parthasarathy, V., Lamzin, V. S., Weiss, M. S. & Tucker, P. A. (2005). *Acta Cryst.* D**61**, 449–457.

Pedersen, K., Christensen, S. K. & Gerdes, K. (2002). *Mol. Microbiol.* **45**, 501–510.

Pedersen, K., Zavialov, A. V., Pavlov, M. Y., Elf, J., Gerdes, K. & Ehrenberg, M. (2003). *Cell*, **112**, 131–140.

Sheldrick, G. M. (2008). *Acta Cryst.* A**64**, 112–122.

Smith, J. A. & Magnuson, R. D. (2004). *J. Bacteriol.* **186**, 2692–2698.

Suzuki, M., Zhang, J., Liu, M., Woychik, N. A. & Inouye, M. (2005). *Mol. Cell*, **18**, 253–261.

Szekeres, S., Dauti, M., Wilde, C., Mazel, D. & Rowe-Magnus, D. A. (2007). *Mol. Microbiol.* **63**, 1588–1605.

Takagi, H., Kakuta, Y., Okada, T., Yao, M., Tanaka, I. & Kimura, M. (2005). *Nature Struct. Mol. Biol.* **12**, 327–331.

Vagin, A. & Teplyakov, A. (1997). *J. Appl. Cryst.* **30**, 1022–1025.

Zhang, Y., Zhang, J., Hoeflich, K. P., Ikura, M., Qing, G. & Inouye, M. (2003). *Mol. Cell*, **12**, 913–923.

Zhang, Y., Zhang, J. & Inouye, M. (2003). *J. Biol. Chem.* **278**, 32300–32306.